PHOTONICS Research

Passively *Q*-switched erbium doped fiber laser using a gold nanostars based saturable absorber

ZHE KANG,[1,2] MINGYI LIU,[2] ZHENWEI LI,[1] SIQING LI,[2] ZHIXU JIA,[2] CHENGZHI LIU,[1] WEIPING QIN,[2] AND GUANSHI QIN[2,*]

[1]*Changchun Observatory, NAO, Chinese Academy of Sciences, Changchun 130012, China*
[2]*State Key Laboratory on Integrated Optoelectronics, College of Electronic Science & Engineering, Jilin University, Changchun 130012, China*
*Corresponding author: qings@jlu.edu.cn

In this paper, we propose and demonstrate an all-fiber passively *Q*-switched erbium doped fiber laser (EDFL) by using gold nanostars (GNSs) as a saturable absorber (SA) for the first time, to the best of our knowledge. In comparison with other gold nanomorphologies, GNSs have multiple localized surface plasmon resonances, which means that they can be used to construct wideband ultrafast pulse lasers. By inserting the GNS SA into an EDFL cavity pumped by a 980 nm laser diode, a stable passively *Q*-switched laser at 1564.5 nm was achieved for a threshold pump power of 40 mW. By gradually increasing the pump power from 40 to 120 mW, the pulse duration decreases from 12.8 to 5.3 µs and the repetition rate increases from 10 to 17 kHz. Our results indicate that the GNSs are a promising SA for constructing pulse lasers.   © 2018 Chinese Laser Press

OCIS codes: (140.3510) Lasers, fiber; (140.3540) Lasers, *Q*-switched; (160.4236) Nanomaterials; (310.6860) Thin films, optical properties.

https://doi.org/10.1364/PRJ.6.000549

1. INTRODUCTION

During the last decade, *Q*-switched fiber lasers have found wide and important applications in the fields of spectroscopy, fiber sensing, material processing, and biomedical diagnostics owing to their large energy pulses, low cost, compactness, and so on [1–5]. Traditionally, the passive *Q*-switched technique based on saturable absorbers (SAs) is one of the most efficient methods for achieving pulsed lasers [6–16]. Semiconductor SA mirrors (SESAMs) are the most commonly used SA for constructing passively *Q*-switched fiber lasers [6]. However, they have limited operation bandwidths (a few tens of nanometers), and their fabrication procedures are very complex [17–19]. Hence, developing new SAs for *Q*-switched lasers plays an important role in ultrafast photonics and related applications.

In recent years, gold nanomaterials, including gold nanoparticles (GNPs) and gold nanorods (GNRs), have been proposed as SAs for constructing *Q*-switched fiber lasers owing to their outstanding optical properties including large third-order nonlinearity, broadband absorption, and fast response, which arise mainly from the localized surface plasmon resonance (SPR) [20–24]. SPR is an optical phenomenon related to the coherent oscillations of electron plasmas at the surfaces of metallic particles. A most important advantage of gold nanomaterials is that variable SPR absorption peaks can be achieved by controlling the morphology and structure of the nanomaterials. In our previous papers, we experimentally demonstrated passively *Q*-switched erbium doped fiber lasers (EDFLs) by using filmy GNPs and GNRs as SAs [20,21]. Fan *et al.* have reported a passively *Q*-switched EDFL using evanescent field interaction with a GNPs SA [22]. In addition, passively *Q*-switched fiber lasers at 635 nm using filmy GNPs as SAs and at 1 µm waveband using filmy GNRs as SAs have also been experimentally demonstrated [23,24]. These results indicate that gold nanomaterials are promising SAs for ultrafast pulse generation. However, the investigation of gold nanomaterials in pulse-laser fields in both theory and experiment is still at the basic level. Thus, there is always a strong motivation to search for high-quality gold nanomaterials with nonlinear saturable absorption effects for pulsed laser generation.

Very recently, a new type of gold nanomaterial, gold nanostars (GNSs), have attracted intensive attention and been applied to surface-enhanced Raman scattering and photothermal therapy due to the unique SPR characteristics [25–32]. The SPR of the GNSs arises from the hybridization of plasmons associated with the core and the individual tips of the particle. The optical properties of the GNSs were found to be highly anisotropic and to strongly depend on the size of the protruding tips. In comparison with other gold

nanomaterials, GNSs have multiple SPR absorption peaks. One is the short wavelength SPR absorption peak with a weak absorption peak around 530 nm, originating from the core plasmons. The others are long wavelength SPRs, which are primarily composed of tip plasmons but with a finite contribution of the core plasmons [27]. The absorption peaks can be tuned in a wide range by varying the morphologies and number of the tips. In addition, the response sensitivity of the long wavelength resonances in GNSs is about 5, much higher than other gold nanomorphologies (0.6 for spheres, 1.5 for nanocubes, and 2.6 for nanorods), and the electron–phonon relaxation time of GNSs is 3.1 ps [30,31]. These results showed that GNSs have fast response and wide absorption bands, indicating that they can be used to construct wideband ultrafast pulsed lasers. However, pulsed laser generation by using GNSs as SAs has not yet been demonstrated experimentally.

In this paper, we propose and demonstrate an all-fiber passively *Q*-switched EDFL by using GNSs as SAs for the first time, which achieves output pulses at 1564.5 nm pumped via a 980 nm laser diode for a pump power of 40 mW. By gradually increasing the pump power from 40 to 120 mW, the pulse duration decreases from 12.8 to 5.3 μs and the repetition rate increases from 10 to 17 kHz. Our results indicate that the GNSs are a promising SA with the potential for important applications in the field of pulsed lasers.

2. PREPARATION AND CHARACTERIZATION OF THE GNS SA

The GNS sample was provided by Nanjing XF NANO Materials Tech Co., Ltd. Figure 1(a) presents a typical transmission electron microscope (TEM) image of the fabricated GNSs, which was measured with a TEM (FEI, F20). The scale bar is 100 nm. About 65 particles of the synthesized GNSs sample were shown in Fig. 1(a). More than 70% of the particles are GNSs, and only a small fraction of other nanomorphologies exists in the sample. The inset in Fig. 1(a) shows the photographs of GNS aqueous solutions and the TEM image of GNSs at a scale of 20 nm. The color of the solution is blue-green, and the diameter of the GNS is about 40 nm. In order to investigate the absorption characteristic at Er^{3+} laser emission waveband (1.56 μm), the absorption spectrum of GNSs was measured with a filmy sample to avoid the strong absorption between 1.4 and 2.1 μm of liquid water. The filmy

sample was prepared by mixing 1 mL GNSs solution and 1 mL 0.2 M (1 M = 1 mol/L) sodium carboxymethylcellulose aqueous solution and casting the mixing solution onto a flat quartz glass substrate, followed by a slow drying at room temperature. We also gave a scanning electron microscope (SEM) characterization (FEI, XL-30) of the GNS film at a scale of 500 nm, as shown in Fig. 1(b). It can be seen that most of GNSs with different numbers of tips are obviously aggregated. The inset in Fig. 1(b) shows the photograph of the GNS film; the color of the film is dark green. Figure 2 shows the absorption spectra of the GNS solution (red line) and GNS film (black line) measured with an UV–visible–near infrared (NIR) spectrophotometer (UV-3600, Shimadzu). It can be seen that the GNS solution has two SPR peaks. The weak, short wavelength SPR peak at 517 nm is caused by the core plasmons, and the strong, long wavelength SPR peak at 655 nm is primarily caused by the tip plasmons but with a finite contribution of the core plasmons. Different from the absorption spectrum of the GNS solution, the GNS film has multiple SPR peaks. The weak, short wavelength SPR peak at 544 nm is also caused by the core plasmons, and the strong, long wavelength SPR peak at 710 nm is also primarily caused by the tip plasmons but with a finite contribution of the core plasmons. Compared with those of the GNS solution, the absorption peaks of GNS film are redshifted. In addition, the long wavelength SPR band also can extend over 1600 nm, which may be caused by the aggregation of GNSs with different morphologies and numbers of the tips [20].

In order to investigate the saturable absorption properties of the GNS SA at 1.56 μm, the dependence of the transmittance on the incident pump peak power density was also characterized by balanced twin detector measurement technology, as shown in Fig. 3. The pump laser used for saturable absorption measurement is a home-made mode-locked EDFL (central wavelength: ~1560 nm, repetition rate: ~35 MHz, pulse duration: ~600 fs). The measured results are presented in Fig. 4. The measurement was performed first by increasing the input power and then by decreasing the input power. The two measurement results are nearly unchanged, which confirms the existence of saturable absorption in GNS SA. By fitting the data shown in Fig. 4 with the equation $\alpha(I) = \alpha_s/(1 + I/I_s) + \alpha_{ns}$ [where $\alpha(I)$ is the absorption coefficient; α_s and α_{ns} are
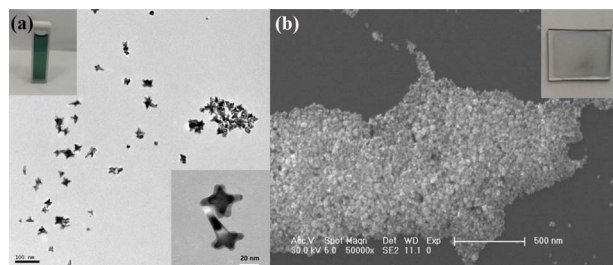

Fig. 1. Characterization of the GNSs and GNS film. (a) TEM image of GNSs at scale of 100 nm; inset: photographs of GNS aqueous solution and the TEM image of GNSs at a scale of 20 nm. (b) SEM image of GNS film at scale of 500 nm; inset: the photograph of GNS film.
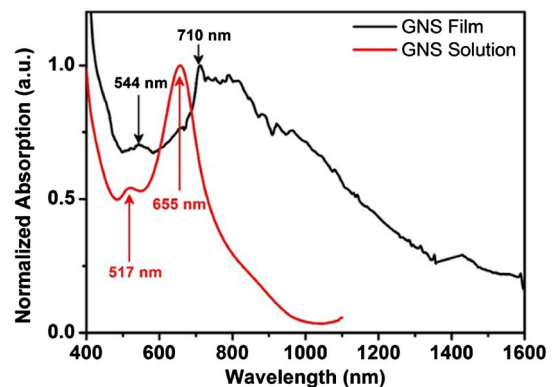

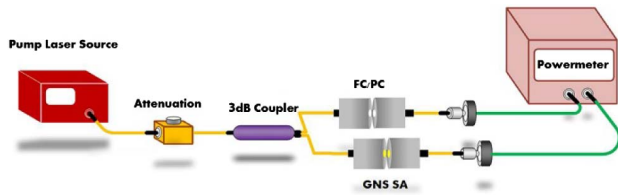**Fig. 2.** Absorption spectra of GNS solution (red line) and GNS film (black line).

Fig. 3. Setup of measurement of saturable absorption by balanced twin detector measurement technology.
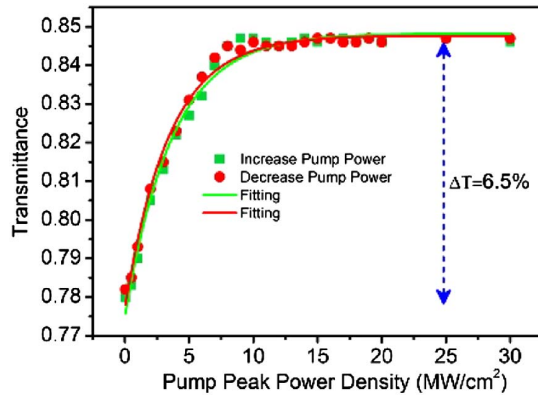

Fig. 4. Dependence of the transmittance of the GNS film on the incident pump peak power density.

the saturable and nonsaturable absorption components, respectively; and I and I_s are input and saturation intensities, respectively], the modulation depth, nonbleachable loss, and saturation intensity were determined to be ~6.5%, ~15.3%, and ~11.8 MW/cm^2, respectively. These results showed that the GNS SA could be used to construct passively Q-switched fiber lasers at 1.56 μm.

3. LASER EXPERIMENT AND RESULTS

The experimental setup for the passively Q-switched EDFL by using GNSs as SA is shown in Fig. 5. A 20 cm long erbium doped fiber (Thorlabs, 24.5 ps^2/km) is pumped by a 980 nm
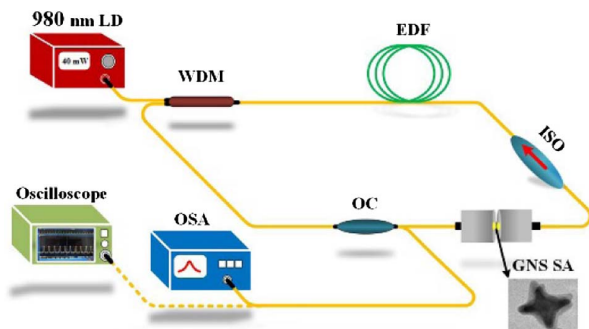

Fig. 5. Schematic of the experimental setup for the GNS based passively Q-switched EDFL. Laser diode (LD), wavelength division multiplexer (WDM), Er^{3+} doped fiber (EDF), isolator (ISO), output coupler (OC), optical spectrum analyser (OSA). Inset: TEM image of GNS.

laser diode through a 980/1550 nm wavelength division multiplexing (WDM) coupler. Undirectional laser operation was guaranteed by adding an isolator in the laser cavity. The GNS SA was put into the laser cavity for inducing Q-switched operation. The insert loss of the GNS SA was about ~0.8 dB. The laser output was extracted via a 10 dB output coupler. The rest of the fibers in the laser ring cavity are single-mode fibers with a dispersion of –18 ps^2/km at 1560 nm, and the total length of the cavity is 6 m. The total dispersion of the cavity is about –0.0995 ps^2 at 1560 nm. The Q-switched lasers were analyzed by using an optical spectrum analyzer (YOKOGAWA, AQ6375), a digital oscilloscope (Tektronix, DPO4108B) together with a photodetector (Newport, 818-BB-51F), and a power meter.

Continuous wave (CW) laser operation started when the incident pump power was increased to 30 mW, and passively Q-switched laser oscillation was achieved as soon as the incident pump power exceeded the threshold of 40 mW. Figure 6 summarizes the typical characteristics of the Q-switching operation at 120 mW. Figure 6(a) shows the emission spectra of the CW laser and Q-switched laser. The operating central wavelength is about 1564.5 nm. Compared to the CW laser, the spectrum of the Q-switched laser shows obvious broadening. Figures 6(b) and 6(c) show the pulse train and single pulse profile of the Q-switched EDFL, respectively. The interval between two adjacent pulses is about 58.8 μs, corresponding to a repetition rate of 17 kHz. The duration of a single pulse width is 5.3 μs, which can be further reduced by reducing the length of the laser cavity [33]. The pulse repetition rate and the pulse duration as a function of the incident pump power were recorded as shown in Fig. 6(d). By varying the pump power from 40 to 120 mW, the pulse duration reduced from 12.8 to 5.3 μs and the repetition rate increased from 10 to 17 kHz, exhibiting the typical feature of passive Q-switching [20,21]. Note that SAs could be overblanched at higher pump intensity; this may lead the pulse to be unstable. The Q-switched fiber laser exhibited an excellent stability at room temperature. In order to confirm the long-term stability
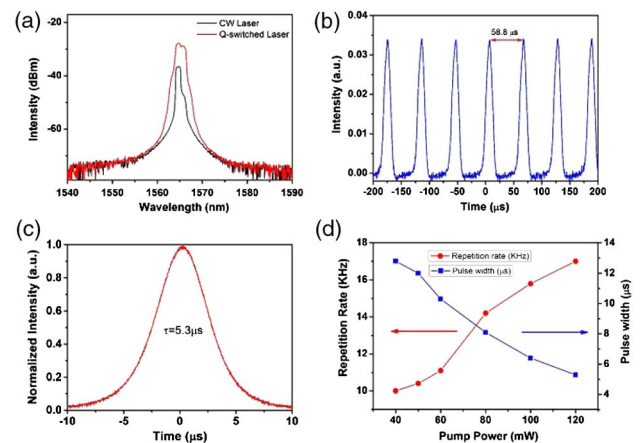

Fig. 6. Q-switched pulse output characterization in the EDF laser cavity with a GNS SA. (a) Optical spectra of CW laser and Q-switched pulsed laser. (b) Pulse train and (c) single pulse characteristics of Q-switched pulsed laser for a pump power of 120 mW. (d) Pulse repetition rate and pulse width versus pump power.
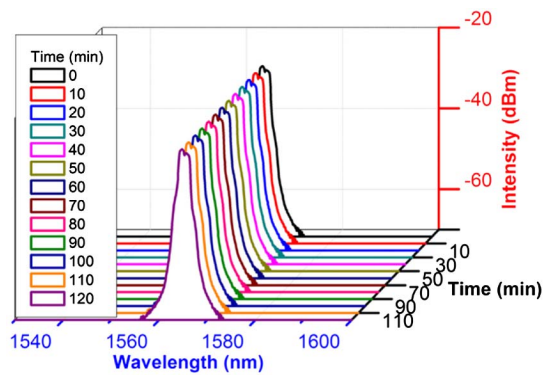
Fig. 7. Measured emission spectra of the *Q*-switched laser based on the GNS SA.

of GNSs as SA, we measured the emission spectrum of the *Q*-switched laser based on GNS SA every 10 min for 2 h. The emission spectra are shown in Fig. 7; neither the central wavelength nor output power is varied. These results showed that the GNS SA is stable for constructing *Q*-switched lasers.

The relationship between the average output powers and pump powers is shown in Fig. 8. The maximum average output power of 2.1 mW was achieved under the pump power of 120 mW, corresponding to a slope efficiency of 1.9%. The low slope efficiency was mainly caused by the low output ratio of the output coupler. Only 10% of the total power was extracted from the laser cavity. In the future, we will increase the output ratio through changing the output coupler, in order to improve the slope efficiency. The maximum pulse energy is about 0.12 µJ. In addition, the *Q*-switched EDFL became unstable when the pump power was larger than 120 mW. The SA might be damaged due to the photothermal effect occurring in GNSs [34]. To overcome this effect, an effective way is to explore the new fabrication methods of SA devices, such as using the evanescent effect through the composite GNSs with microfiber [12,17]. This can enlarge the interactive areas between pump light and GNS materials, further reducing the photothermal effects of the GNSs SA. Further work will be done for increasing the damage threshold by using microfiber-based SAs [35,36].
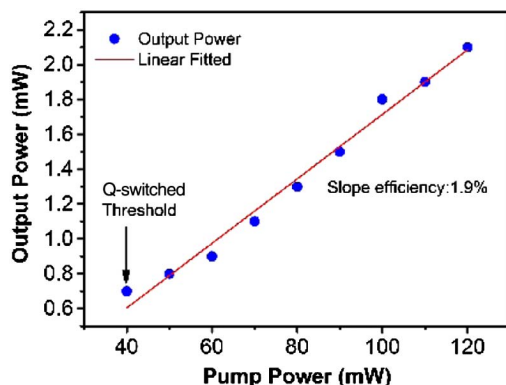
Lifetime of the SA is a key factor for practical applications. In order to confirm the lifetime of GNSs as SA, we measured the performance of the *Q*-switched fiber laser based on GNSs SA every three days for almost two months. The threshold of *Q*-switched laser operation did not have any change, and neither the central wavelength nor output power was varied, which shows that the long term stability of GNS SA is good for real applications.

In addition, although the GNS film has a broad absorption band, we have not realized pulse laser operation at other wavelengths up to now, due to the different mechanisms of the laser generation at different wavelengths. In the future, we will try to realize the mode-locked or *Q*-switched lasers at different wavelengths, in order to make the best use of the broadband saturable absorption of GNSs.

4. CONCLUSION

In conclusion, we have experimentally demonstrated an all-fiber passively *Q*-switched EDFL by using GNSs as a SA. The long wavelength SPR band can extend over 1600 nm, which may be caused by the aggregation of GNSs with different morphologies and number of the tips. By inserting the GNSs SA into the EDFL cavity, stable passively *Q*-switched laser at 1564.5 nm was achieved for a threshold pump power of 40 mW. By gradually increasing the pump power from 40 to 120 mW, the pulse duration decreases from 12.8 to 5.3 µs and the repetition rate increases from 10 to 17 kHz. The obtained results indicate that the GNS SA can be used for constructing pulsed lasers.

Fig. 8. Relationship between the average output powers and pump powers.

REFERENCES

1. D. Popa, Z. Sun, T. Hasan, F. Torrisi, F. Wang, and A. C. Ferrari, "Graphene *Q*-switched, tunable fiber laser," Appl. Phys. Lett. **98**, 073106 (2011).
2. C. Sobon, J. Sotor, J. Jagiello, R. Kozinski, K. Librant, M. Zdrojek, L. Lipinska, and K. M. Abramski, "Linearly polarized, *Q*-switched Er-doped fiber laser based on reduced graphene oxide saturable absorber," Appl. Phys. Lett. **101**, 241106 (2012).
3. V. N. Filippov, A. N. Starodumov, and A. V. Kir'yanov, "All-fiber passively *Q*-switched low-threshold erbium laser," Opt. Lett. **26**, 343–345 (2001).
4. D. P. Zhou, L. Wei, B. Dong, and W. K. Liu, "Tunable passively switched erbium-doped fiber laser with carbon nanotubes as a saturable absorber," IEEE Photon. Technol. Lett. **22**, 9–11 (2010).
5. W. Shi, Q. Fang, X. S. Zhu, R. A. Norwood, and N. Peyghambarian, "Fiber lasers and their applications," Appl. Opt. **53**, 6554–6568 (2014).
6. O. Okhotnikov, A. Grudinin, and M. Pessa, "Ultra-fast fiber laser systems based on SESAM technology: new horizons and applications," New J. Phys. **6**, 177 (2004).

7. U. Keller, "Recent development in compact ultrafast lasers," Nature **424**, 831–838 (2003).

8. J. F. Li, H. Y. Luo, B. Zhai, R. G. Lu, Z. N. Guo, H. Zhang, and Y. Liu, "Black phosphorus: a two-dimension saturable absorption material for mid-infrared *Q*-switched and mode-locked fiber lasers," Sci. Rep. **6**, 30361 (2016).

9. R. W. Zhao, J. L. He, X. C. Su, Y. R. Wang, X. L. Sun, H. K. Nie, B. T. Zhang, and K. J. Yang, "Tunable high-power *Q*-switched fiber laser based on BP-PVA saturable absorber," IEEE J. Sel. Top. Quantum Electron. **24**, 0900405 (2018).

10. Z. Q. Wang, L. Zhan, M. L. Qin, J. Wu, L. Zhang, Z. X. Zou, and K. Qian, "Passively *Q*-switched Er-doped fiber laser using alcohol," J. Lightwave Technol. **33**, 4857–4861 (2015).

11. J. Koo, J. Lee, W. Shin, and J. H. Lee, "Large energy, all-fiberized *Q*-switched pulse laser using a GNRs/PVA saturable absorber," Opt. Mater. Express **5**, 1859–1867 (2015).

12. X. D. Wang, Z. C. Luo, M. Liu, M. Liu, Y. L. Qi, R. Tang, A. P. Luo, and W. C. Xu, "A microfiber-based gold nanorod saturable absorber with evanescent field interaction for multi-soliton patterns in a fiber laser," Laser Phys. **26**, 065105 (2016).

13. Q. L. Bao, H. Zhang, Y. Wang, Z. H. Ni, Y. L. Yan, Z. X. Shen, K. P. Loh, and D. Y. Tang, "Atomic-layer graphene as a saturable absorber for ultrafast pulsed lasers," Adv. Funct. Mater. **19**, 3077–3083 (2009).

14. Z. P. Sun, T. Hasan, F. Torrisi, D. Popa, G. Privitera, F. Q. Wang, F. Bonaccorso, D. M. Basko, and A. C. Ferrari, "Graphene mode-locked ultrafast laser," ACS Nano **4**, 803–810 (2010).

15. S. Yamashita, "A tutorial on nonlinear photonic applications of carbon nanotube and graphene," J. Lightwave Technol. **30**, 427–447 (2012).

16. C. Zhao, H. Zhang, X. Qi, Y. Chen, Z. Wang, S. Wen, and D. Tang, "Ultra-short pulse generation by a topological insulator based saturable absorber," Appl. Phys. Lett. **101**, 211106 (2012).

17. Z. C. Luo, M. Liu, Z. N. Guo, X. F. Jiang, A. P. Luo, C. J. Zhao, X. F. Yu, W. C. Xu, and H. Zhang, "Microfiber-based few-layer black phosphorus saturable absorber for ultra-fast fiber laser," Opt. Express **23**, 20030–20039 (2015).

18. Y. H. Xu, Z. T. Wang, Z. N. Guo, H. Huang, Q. L. Xiao, H. Zhang, and X. F. Yu, "Solvothermal synthesis and ultrafast photonics of black phosphorus quantum dots," Adv. Opt. Mater. **4**, 1223–1229 (2016).

19. H. R. Mu, Z. T. Wang, J. Yuan, S. Xiao, C. Y. Chen, Y. Chen, Y. Chen, J. C. Song, Y. S. Wang, Y. Z. Xue, H. Zhang, and Q. L. Bao, "Graphene-Bi$_2$Te$_3$ heterostructure as saturable absorber for short pulse generation," ACS Photon. **2**, 832–841 (2015).

20. T. Jiang, Y. Xu, Q. J. Tian, L. Liu, Z. Kang, R. Y. Yang, G. S. Qin, and W. P. Qin, "Passively *Q*-switching induced by gold nanocrystals," Appl. Phys. Lett. **101**, 151122 (2012).

21. Z. Kang, X. Y. Guo, Z. X. Jia, Y. Xu, L. Liu, D. Zhao, G. S. Qin, and W. P. Qin, "Gold nanorods as saturable absorbers for all-fiber passively *Q*-switched erbium-doped fiber laser," Opt. Mater. Express **3**, 1986–1991 (2013).

22. D. Fan, C. Mou, X. Bai, S. Wang, N. Chen, and X. Zeng, "Passively *Q*-switched erbium-doped fiber laser using evanescent field interaction with gold-nanosphere based saturable absorber," Opt. Express **22**, 18537–18542 (2014).

23. X. D. Wang, Z. C. Luo, H. Liu, N. Zhao, M. Liu, Y. F. Zhu, J. P. Xue, A. P. Luo, and W. C. Xu, "Gold nanorods as saturable absorber for *Q*-switched Yb-doped fiber laser," Opt. Commun. **346**, 21–25 (2015).

24. D. Wu, J. Peng, Z. Cai, J. Weng, Z. Luo, N. Chen, and H. Xu, "Gold nanoparticles as a saturable absorber for visible 635 nm *Q*-switched pulse generation," Opt. Express **23**, 24071–24076 (2015).

25. Z. Kang, Q. Li, X. J. Gao, L. Zhang, Z. X. Jia, Y. Feng, G. S. Qin, and W. P. Qin, "Gold nanorod saturable absorber for passive mode-locking at 1 μm wavelength," Laser Phys. Lett. **11**, 035102 (2014).

26. Z. Kang, Y. Xu, L. Zhang, Z. X. Jia, L. Liu, D. Zhao, Y. Feng, G. S. Qin, and W. P. Qin, "Passively mode-locking induced by gold nanorods in erbium-doped fiber lasers," Appl. Phys. Lett. **103**, 041105 (2013).

27. H. Feng, L. Colleen, H. Jason, and N. Peter, "Plasmon resonances of a gold nanostar," Nano Lett. **7**, 729–732 (2007).

28. G. G. Khoury and T. Vo-Dinh, "Gold nanostars for surface-enchanced Raman scattering: synthesis, characterization and optimization," J. Phys. Chem. C **112**, 18849–18859 (2008).

29. S. K. Dondapati, T. K. Sau, C. Hrelescu, T. A. Klar, F. D. Stefani, and J. Feldmann, "Label-free biosensing based on single gold nanostars as plasmonic transducers," ACS Nano **4**, 6318–6322 (2010).

30. Y. Hua, K. Chandra, D. M. Dam, G. P. Wiederrecht, and T. W. Odom, "Shape-dependent nonlinear optical properties of anisotropic gold nanoparticles," J. Phys. Chem. Lett. **6**, 4904–4908 (2015).

31. P. S. Kumar, I. Pastoriza-Santos, B. Rodriguez-Gonzalez, F. J. Garcia de Abajo, and L. M. Liz-Marzan, "High-yield synthesis and optical response of gold nanostars," Nanotechnology **19**, 015606 (2008).

32. H. Yuan, A. M. Fales, and T. Vo-Dinh, "TAT peptide-functionalized gold nanostars: enhanced intracellular delivery and efficient NIR photothermal therapy using ultralow irradiance," J. Am. Chem. Soc. **134**, 11358–11361 (2012).

33. J. Liu, S. Wu, Q. H. Yang, and P. Wang, "Stable nanosecond pulse generation from a grapheme-based passively *Q*-switched Yb-doped fiber laser," Opt. Lett. **36**, 4008–4010 (2011).

34. X. Chen, Y. T. Chen, M. Yan, and M. Qiu, "Nanosecond photothermal effects in plasmonic nanostructures," ACS Nano **6**, 2550–2557 (2012).

35. X. D. Wang, Z. C. Luo, H. Liu, M. Liu, A. P. Luo, and W. C. Xu, "Microfiber-based gold nanorods as saturable absorber for femtosecond pulse generation in a fiber laser," Appl. Phys. Lett. **105**, 161107 (2014).

36. N. H. Park, H. Jeong, S. Y. Choi, M. H. Kim, F. Rotermund, and D. Yeom, "Monolayer graphene saturable absorbers with strongly enhanced evanescent-field interaction for ultrafast fiber laser mode-locking," Opt. Express **23**, 19806–19812 (2015).